http://dx.doi.org/10.15576/GLL/2022.4.7

GLL

Geomatics, Landmanagement and Landscape No. 4 • 2022, 7–26

A COMBINED FIELD AND AUTOMATIC APPROACH FOR LITHOLOGICAL DISCRIMINATION IN SEMI-ARID REGIONS, THE CASE OF GEOLOGICAL MAPS OF BIR LATER REGION AND ITS VICINITY, NEMENTCHA MOUNTS, ALGERIA

Abdelmouhcene Chibani, Riheb Hadji, Hamed Younes

Summary

The Sahara's Nememcha mountains chain suffers from a significant lack of large-scale geological information. In the Bir Later region with complex morpho-structural settings and arid climate conditions; geological maps have not been yet completed by competent authorities. However, this region harbours Algeria's largest phosphate mine; with its reserves estimated at more than one billion tons of ore grading 20% phosphorus pentoxide. Geomatic-based techniques of Multi-source Remote Sensing data allow the classification and identification of the lithologic features. The adopted method quarries the spectral signal, the alteration processes, and the thickness of the rocky banks. For this task, we apply Principal Component Analysis (PCA), Minimum Noise Fraction (MNF), directional filters, and unsupervised classification (K-Means data) techniques to calibrate and correct Landsat 8 OLI and Sentinel-2A multispectral images. A petrographic study with field and laboratory work was carried out in order to confirm the machine description of the different facies. The results showed that the proposed lithology classification scheme can achieve accurate classification of all lithologic types, in the Cenozoic, Mesozoic, and Holocene deposits of the study area. The lithological map obtained from the GIS-RS-Processing is highly correlated with our field survey. Therefore, multispectral image data (Landsat 8 OLI and Sentinel-2A) coupled with an advanced image enhancement technique and field surveys are recommended as a rapid and cost-effective tool for lithologic discrimination and mapping. The experimental results fully demonstrated the advantages of the reliance on laboratory tests in the sensed lithology validation in an arid area.

Keywords

Nememcha mountains • PCA • MNF • directional filters • unsupervised classification

1. Introduction

Remote sensing can provide information from Earth observations for lithology discrimination, especially in arid regions where the field survey is hard to carry out [Tamani

et al. 2019]. Compared with traditional techniques based on direct field measurement of rock outcrops, the lithology information aquired from optical remote sensing data is much more capable of capturing geologic information, and can effectively improve the reliability of the obtained terrain information [Lu et al. 2022]. Geological mapping provides a lot of important information about geology in a legible form. They are very useful when making geological [Hadji et al. 2014a, Dahoua et al. 2017], geotechnical [Achour et al. 2017, Anis et al. 2019], hydrogeological [Hamed et al. 2014, Demdoum et al. 2015, Mokadem et al. 2016], mining environment [Zahri et al. 2016], natural hazards mitigation [Hadji et al. 2013, 2014b, El Mekki et al. 2017], and disaster management maps [Hadji et al. 2017a, b, Mouici et al. 2017, Manchar et al. 2018]. The Nememcha mountains, and the Saharan Atlas in general, suffer from a lack of geological data. For this effect, remote sensing allows us to describe the lithology using the spectral signal, the alteration characteristics, the drainage networks, and the thickness of the rocky banks [Tamani et al. 2019].

Our research aims to establish a geological map of the study area based on remote sensing and field data that apply various methods and techniques such as principal component analysis (PCA), minimum noise fraction (MNF), directional filters, and unsupervised classification on Landsat 8 OLI and Sentinel-2A multispectral image data, coupled and validated by field and laboratory work [Shirmard et al. 2022]. The application of processing and classification on these multispectral satellite images are very useful for geological mapping studies and even more so in semi-arid to arid environments with minimal vegetation [El Fels and El Ghorfi 2022].

The methods were chosen for this study based on their effectiveness and ease of application to achieve our objective. The PCA transformation reduces the dimensions of the data without much loss of information, the MNF reconverts the multispectral images with less noise, and the decorrelation stretch removes the high correlation commonly found in multispectral datasets. The K-Means clustering technique is an automatic data classification technique adopted in case of the lack of spectral data on various rocks and facies in the area [Shebl et al. 2022].

2. General settings

Located on the Algerian-Tunisian border, the study area is an arid mountainous terrain. This complex topographic and geologic structure is marked by the Jebel Onk, Jebel Zraga and Jebel Mrata sedimentary massifs (Fig. 1a). The stratigraphic column shows carbonatic facies created between Cretaceous and Holocene (Fig. 1b-c) [N'cibi et al. 2020]. In the Jebel Onk massif, it consists of chemical facies, of 500 m thick, covered in discordance by a thick continental sandy-clayey series of Miocene and then Quaternary age filling the synclinal structures and fossilizing the series of pre-Miocene age (Fig. 1b-c) [Gadri et al. 2015]. Jebel Zraga and Jebel Mrata contain carbonates series of the Upper Cretaceous with a marly series covering syncline troughs. The plains are covered by sandy, marly, clayey and silty formations of the Mio-Plio-Quaternary age [Rais et al. 2017]. From a structural point of view, the Upper Cretaceous to Eocene series of

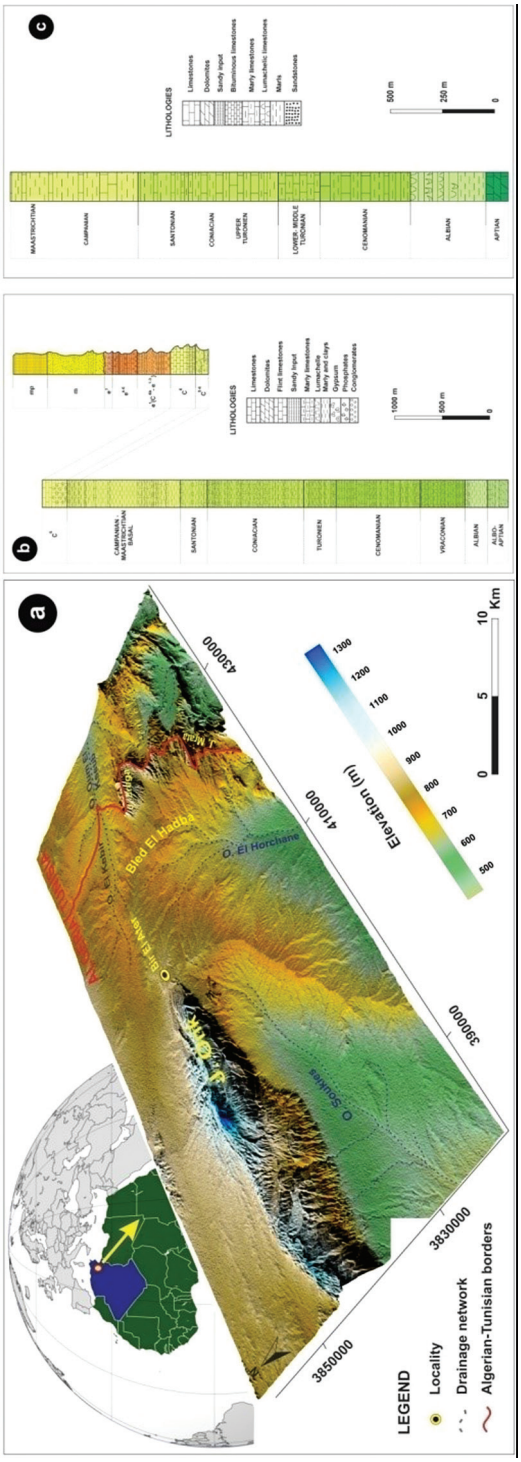

Source: Authors' own study

Fig. 1. a) Geographic location of the study area (Digital Elevation Model SRTM30). b) Stratigraphic log of Cretaceous and Tertiary terrains. c) Core drill DK-1 of Jebel Onk

the Jebel Onk-Metloui basin is structured in a series of asymmetrical anticlines and synclines fractured in their flanks, most often SW-NE and stalled b transverse accidents N°120 to N140° E [Hamed et al. 2017, 2022]. This region is characterized by an arid climate, cold in the winter and very hot in the summer. The hydrographic network consists of three main wadies: Soukies, Horchane and Kebir. (Fig. 1a) [Hamad et al. 2018, 2021].

3. Material and methods

3.1. Data acquisition

For the lithological discrimination, we used the following data:

Landsat 8 OLI images have a spatial resolution of 30 meters per pixel, with the exception of the panchromatic band (band 8) which has a resolution of 15 meters per pixel. These images also have nine spectral bands. Its specifications are presented in Table 1. To cover the study area, we used only one image (LC81920362018357LGN00, Path: 192, Row: 36, date acquired: 23.12.2018), (Fig. 2). Sentinel-2A images downloaded from (https://scihub.copernicus.eu) a website, the Sentinel-2A imagery covers 13 spectral bands in the VNIR and SWIR spectral signal, with four (04) bands with a spatial resolution of 10 m per pixel, six (06) with a spatial resolution of 20 m per pixel, and the remaining three (03) bands with a spatial resolution of 60 m per pixel (Table 1). To cover the study area, we composed two scenes, acquired in: 26.08.2020 (S2A_MSIL2A_T32SLD, S2A_MSIL2A_T32SMD,) (Fig. 2), we also used the ESA-SNAP and ENVI software to process the Sentinel-2A imagery. Then, we download the Shuttle Radar Topography Mission (SRTM) digital elevation model (DEM) with a spatial resolution of 30 m per pixel from the official USGS website (http://earthexplorer.usgs.gov/). We processed the DEM and derivated several thematic layers using the ArcGIS 10.8 software.

We used the geological map and the notice of Bir El Ater (N°327), to interpret and correlate several classifications performed on the Landsat 8 OLI and Sentinel-2A images before confirming these results with field and laboratory work.

The analysis of the Landsat 8 and Sentinel-2A data for lithological discrimination is based on the relationship between spectral absorbance or emittance and the mineral composition of the rock units under investigation.

Table 1. Landsat 8 OLI and Sentinel-2A spectral bands specifications

Image	Resolution	Spectral bands	Wavelength (nm)
Landsat 8 OLI	30 m	**1** – Coastal / Aerosol	0.443
		2 – Blue	0.4826
		3 – Green	0.5613
		4 – Red	0.6546
		5 – Near Infrared (NIR)	0.8646
		6 – Short Wavelength Infrared (SWIR)	1.6090
		7 – Short Wavelength Infrared (SWIR)	2.2010
		9 – Ciruus	1.3730
	15 m	**8** – Panchromatic	0.5917
Sentinel-2A	10 m	**2** – Blue	0.4900
		3 – Green	0.5600
		4 – Red	0.6650
		8 – NIR	0.8420
	20 m	**5** – Vegetation Red Edge	0.7050
		6 – Vegetation Red Edge	0.7400
		7 – Vegetation Red Edge	0.7830
		8a – Vegetation Red Edge	0.8650
		11 – Short Wavelength Infrared (SWIR)	0.1610
		12 – Short Wavelength Infrared (SWIR)	0.2190
	60 m	**1** – Coastal aerosol	0.0.443
		9 – Water Vapour	0.9450
		10 – SWIR – Cirrus	0.1380

Source: Authors' own study

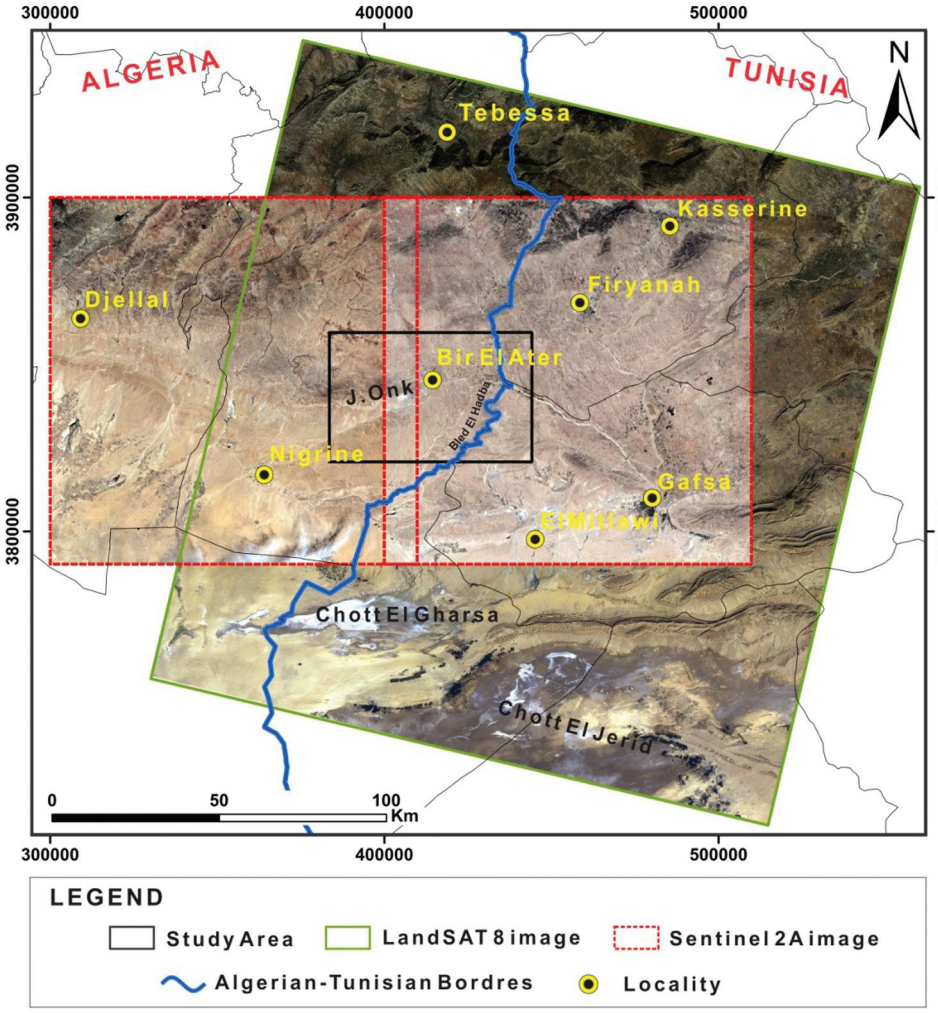

Source: Authors' own study

Fig. 2. Position and names of the satellite images used

3.2. Data Pre-processing

The scene from the Landsat 8 OLI was calibrated atmospherically, and radiometrically at ENVI 5.3. The calibration began with converting the values of Digital Numbers (DN) to Top of Atmosphere (ToA) reflectance, and then to Surface Reflectance (SR).

Both of the Sentinel-2A scenes were corrected atmospherically, radiometrically, and geometrically. The spectral bands 1, 9, and 10 with a spatial resolution of 60 m per pixel were removed. The 5, 6, 7, 8a, 11, and 12 bands were resampled to a spatial resolution

of 10 m per pixel using the Nearest Neighbor method. Then all of the 2, 3, 4, 5, 6, 7, 8, 8a, 11, and 12 bands were stacked to compose the final images scene.

3.3. Data processing

Principal Component Analysis (PCA)

The principal component analysis method is a conventional multivariable statistical analysis approach. Several scientific researchers have successively applied this method in the geosciences field [Khan et al. 2007]. In PCA, a set of correlated variables were converted to a set of linearly uncorrelated variables using an orthogonal transform. The resulting uncorrelated variables are called principal components (PCs). This transformation can reduce the dimensions of data without much loss of information.

Minimum noise fraction (MNF)

This is a noise reduction technique proposed by [Green et al. 1988] to increase the signal-to-noise ratio (SNR). It is widely used for feature extraction, noise whitening, and spectral data reduction of remote sensing imagery [Ge et al. 2018].

It is based on two consecutive operations: 1) the estimation of the noise level in the data as indicated by a correlation matrix. 2) the use of the main elements derived from the results of the first operation.

We used the inverse of MNF (with the correct Digital Numbers "DN") to reconvert the image with less noise. We can use this image for other spectral treatments (classifications or spectral analysis) [Fal et al. 2019].

Decorrelation stretch

Decorrelation stretch is applied to suppress strong correlation commonly found in multispectral data sets. To enhance (stretch) the color differences found in a color image, we use remove the correlation between channels with each pixel [Alley 1999].

Lineament's detection and analysis

Directional filters are used for structural analysis. This technique enhances the perception of lineaments, causing an optical drop shadow effect on the image as if it were illuminated by grazing light [Hammad et al. 2016]. Linear enhancement was performed using directional filters in four directions: N000°, N045°, N090°, and N135°. These filters were applied to the 8-NIR band (0.842 μm, 10 m) with a square matrix of order 3, allowing the identification of geological lineaments and the perception of structural details.

3.4. Unsupervised classification

The K-Means clustering technique is an automatic data classification technique. The main idea is to divide the data into K distinct classes. Each individual is attributed to the nearest class. After all the data has been attributed, the average of each class is calcu-

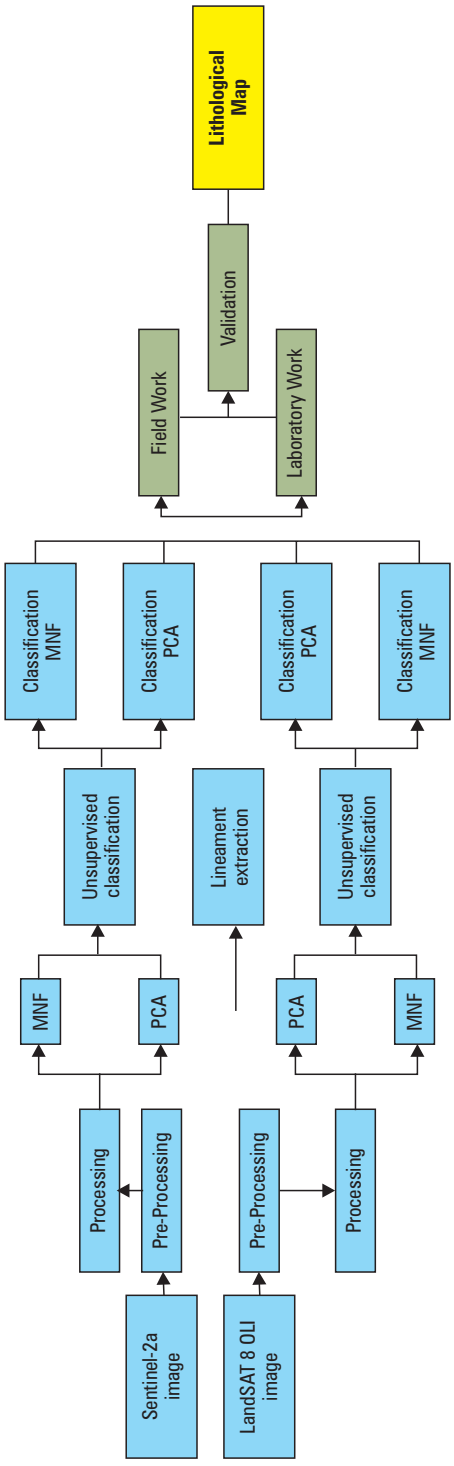

Source: Authors' own study

Fig. 3. Methodological flowchart of the adopted approach

lated and constitutes the new class representatives. When the stationary state is reached (no data change group), the algorithm stops. This process attempts to maximize intra-class similarity represented as an objective function (1):

$$J = \sum_{x=1}^{k} \sum_{xj \in Ci} d(xj - Ci) \tag{1}$$

3.5. Field and laboratory validation

To investigate the accuracy of remotely mapped lithologies, two field checks were implemented in March 2019 and May 2021, and August 2022, respectively. During the first field survey, the lithological units mapped the Algerian-Tunisian border (J. Zraga, El Horchane) were verified and assessed. Rock samples of limestones, dolomitic limestones, lacustrine limestones, and marls were collected. In the second field survey, lithological points and boundaries in the J. Onk complex were visited and assessed. After the field reconnaissance, microscopic study was performed on the collected rock samples. The adopted approach is resumed in the methodological flowchart (Fig. 3)

4. Results and discussions

The digital photo-interpretation was done on the composite colors images of PCA, MNF, the results of directional linear filtering and the unsupervised classification (K-Means) applied to the Sentinel-2A and the Landsat 8 OLI imagery for lithological discrimination in the study area. To discriminate the lithological units, the PCA and MNF methods were applied to the Sentinel-2A and the Landsat 8 OLI images. The first three PCs and MNFs have been more widely adopted for lithological mapping than the subsequent low-order. The first PC and MNF images (PC1 and MNF1) contain the highest percentage of data variance, the second PC and MNF images (PC2 and MNF 2) contain the second highest data variance, in decreasing order, and the last PC image shows almost nothing useful, mere noise, due to the minimum data variance. According to the percentage of data variance in the PCs and MNF images, the PC3, PC2 and PC1 were used to produce a false color composite for lithological discrimination on the Sentinel-2A and the Landsat 8 OLI images (Fig. 4). Each lithofacies is discriminated by a chromo-facies (Table 2).

Table 2. Chromo-facies in the false color images of PCA and MNF processing

Lithofacies	Figures	Chromo-facies
Carbonate formations of Maastrichtian (Upper Cretaceous) and Paleocene	Fig. 4a	Light green and yellow
	Fig. 4b	Blue and purple
	Fig. 4c	Garnet and light bleu
	Fig. 4d	Light yellow

Table 2. cont.

Gypsum formation of Lutetian (Eocene)	Fig. 4a	Pink
	Fig. 4b	Dark blue
	Fig. 4c	Red
	Fig. 4d	Bright blue
Sands, clays and marls (Mio-Pliocene)	Fig. 4a	Bright green
	Fig. 4b	Bright green and yellow
	Fig. 4c	Bright green
	Fig. 4d	Orange and red
Alluviums (Quaternary)	Fig. 4a	White and cream
	Fig. 4b	Leaf green
	Fig. 4c	Light green
	Fig. 4d	Gray

The lineament map resulting from the direct extraction of the lineaments using directional filters in the directions: N000°, N045°, N090°, and N135°, shows that the major geological complexes of the study area are affected by intense fracturing deformation at different scales. It shows a large predominance of roughly NW-SE lineaments in the direction of N110° and N120°, their density is more important in the central part of the anticline of J. Onk and J. Fouris. There are lineaments in the E-W direction, which appear in J. Mrata, J. Fadjennahla, J. Sif Leham (Fig. 5).

An unsupervised classification was carred out in order to highlight the lithological units of the study area. The choice of ten (10) classes is based on the lithology of the map of Bir el Ater N°327, at a scale 1: 50 000. The unsupervised classification "K-Means" was performed on the results of processing (PCA and MNF) of the Landsat 8 OLI and the Sentinel-2A images. The results of the classification (Fig. 6) are almost the same on all of the images. They are well correlated with the existing Bir El Ater mineral map and the validations made on the field.

5. Field and laboratory validation

The lithological succession extending from the Upper Cretaceous to the Quaternary:
Upper Cretaceous: Mainly formed of carbonates and marls with intercalations of small levels of marly limestone. The Maastrichtian is characterized by a metric mass of fractured limestone with a black flint of cream color with a white breakage (Fig. 7a). A lot of *Inoceramus* fossils are found there , as well as of other bivalve shells and gastropods. These carbonates are biomicritic mudstone textures showing rare foraminifera (benthic: *Textularia* sp. Ans *Lenticulina* sp., planktonic: *Hedbergella* sp ...) and bivalve sections.

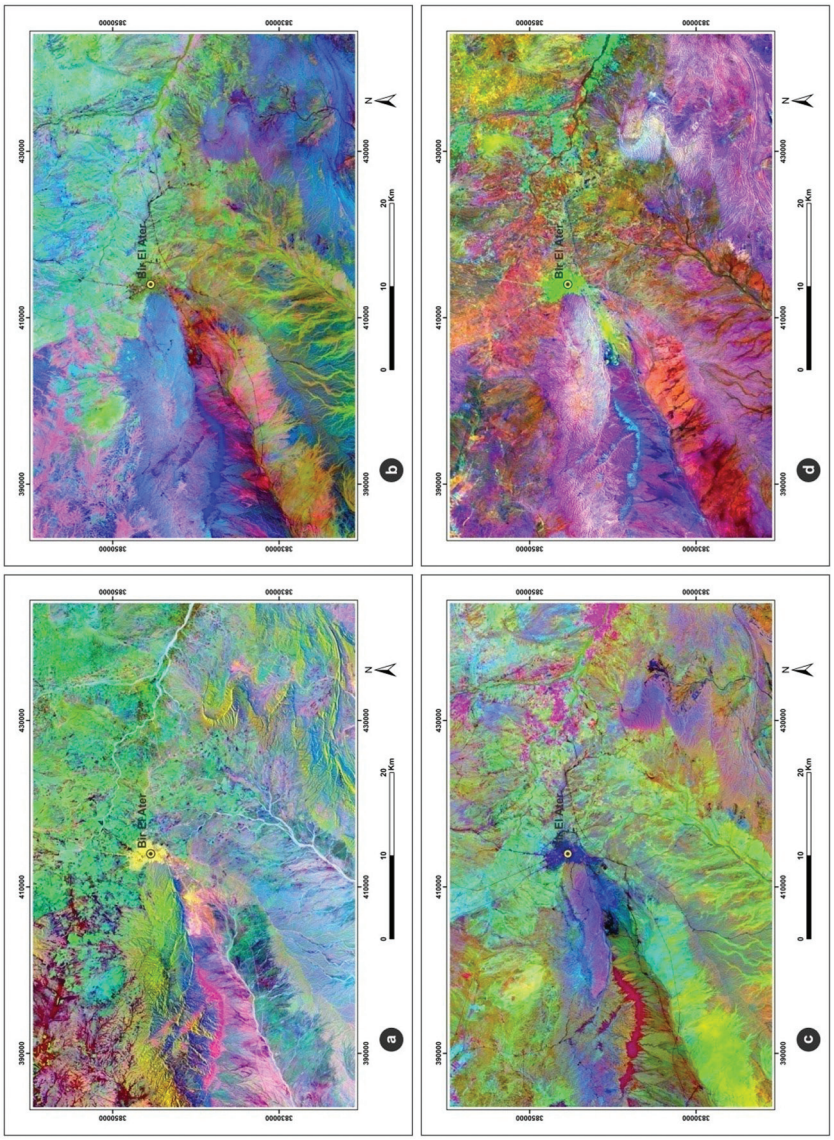

Source: Authors' own study

Fig. 4. False color composite of: a) PCs 3, 2, and 1 of the Landsat 8. b) MNF 3, 2, and 1 of the Landsat 8. c) PCs 3, 2, and 1 of the Sentinel 2A. d) MNF 3, 2, and 1 of the Sentinel 2A

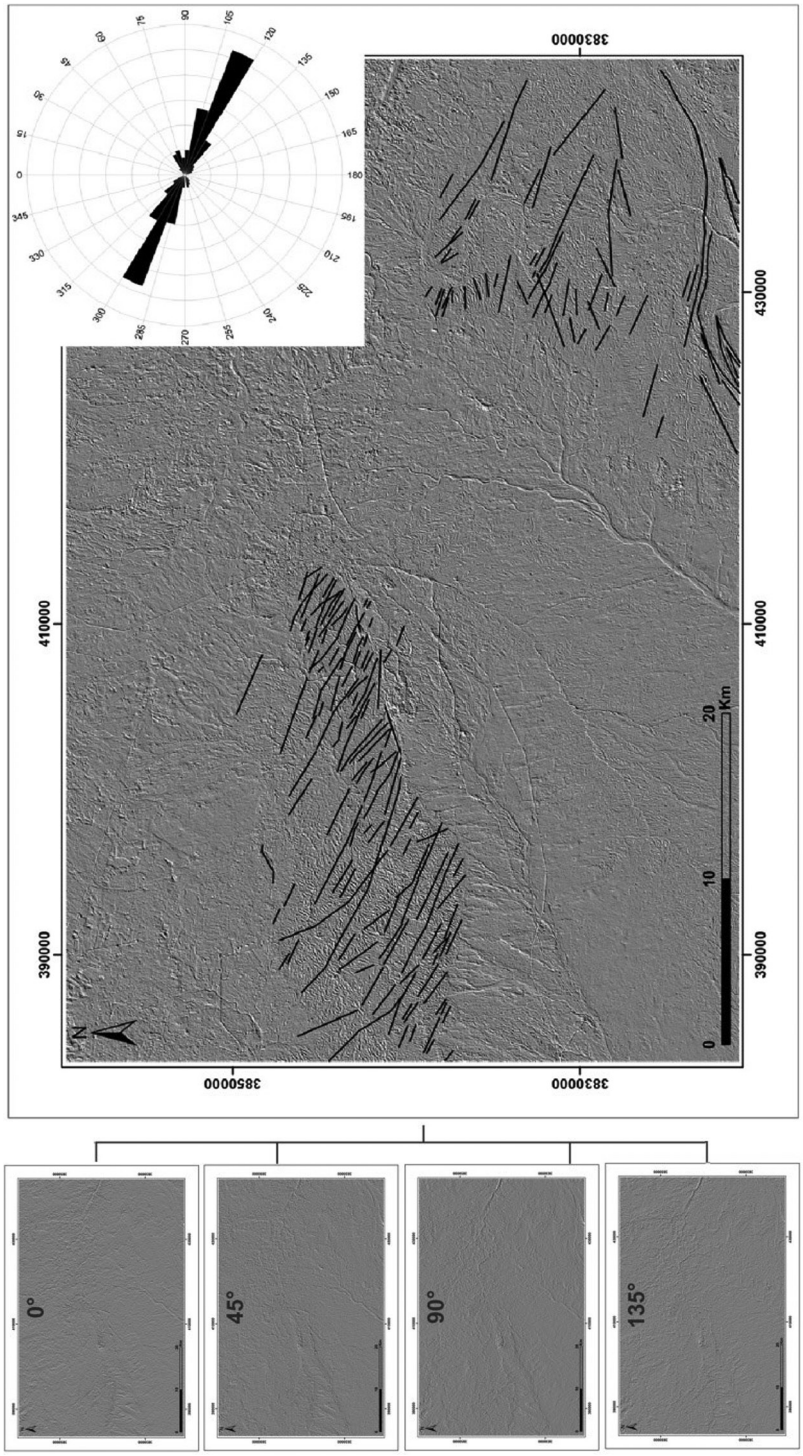

Source: Authors' own study

Fig. 5. Directional filters application and lineaments map of the study area

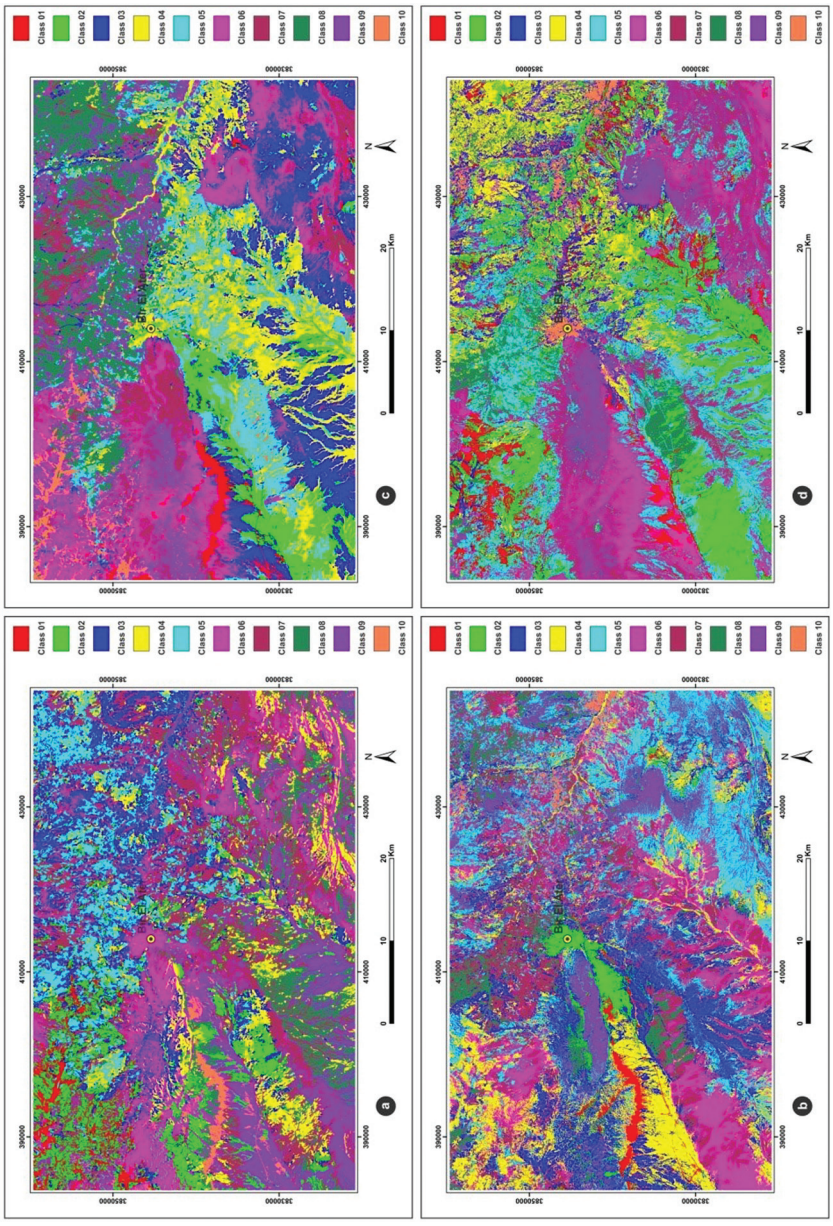

Source: Authors' own study

Fig. 6. K-Means unsupervised classification: a) Landsat 8 PCA (3, 2, and 1. b) Landsat MNF (3, 2, and 1). c) Sentinel 2A PCA (3, 2, and 1). d) Sentinel 2A MNF (3, 2, and 1)

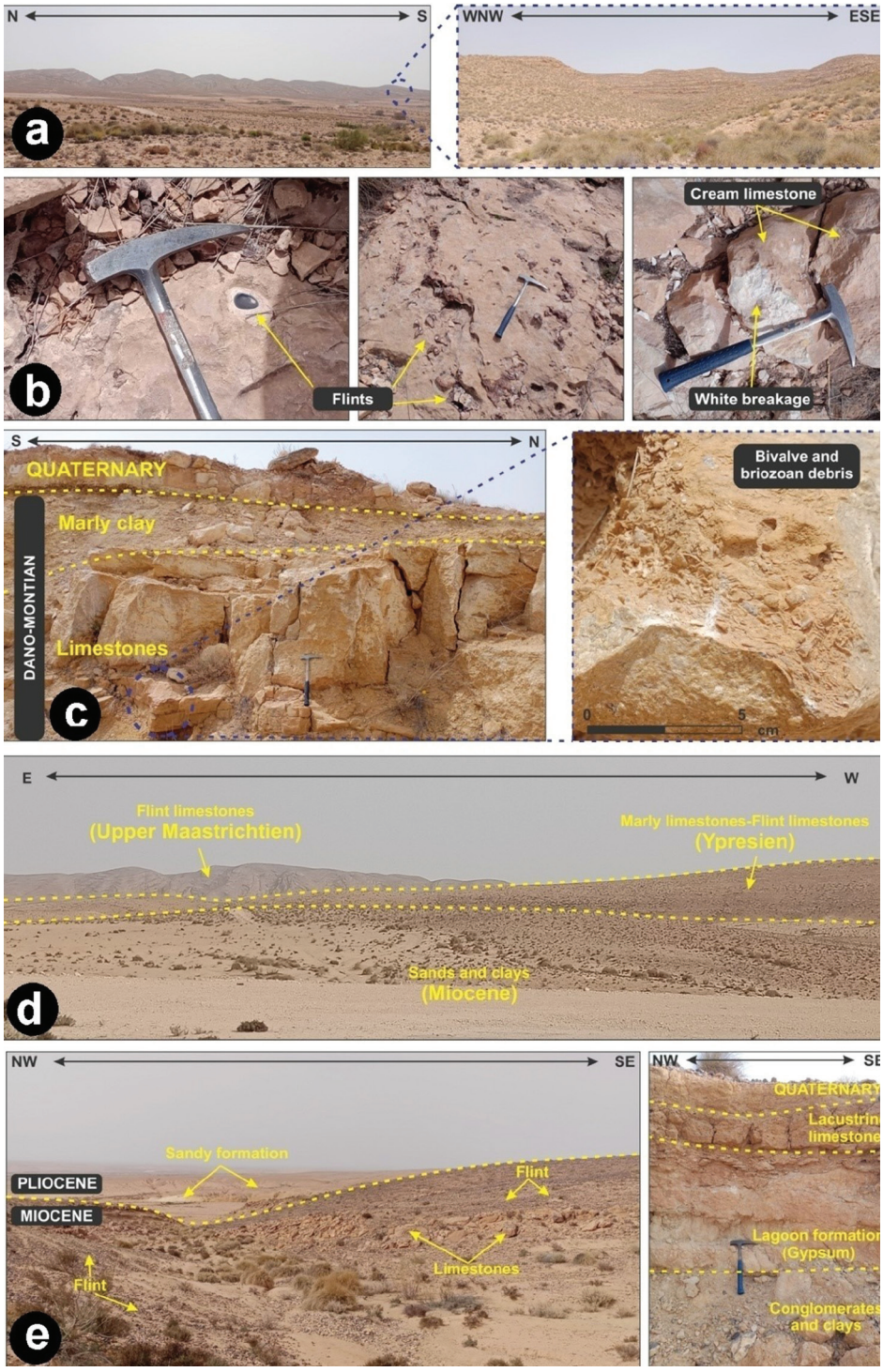
N
S
a
WNW
ESE
b
Flints
Cream limestone
White breakage
S
N
QUATERNARY
Marly clay
DANO-MONTIAN
Limestones
c
Bivalve and
briozoan debris
0
5
cm
E
W
Flint limestones
(Upper Maastrichtien)
Marly limestones-Flint limestones
(Ypresien)
Sands and clays
(Miocene)
d
NW
SE
Sandy formation
PLIOCENE
MIOCENE
Flint
Flint
Limestones
e
NW
SE
QUATERNARY
Lacustrin
limestone
Lagoon formation
(Gypsum)
Conglomerates
and clays

Dano-Montian: Dano-Montian series begins with a carbonate chalk with yellowish-white breakage that is very rich in fauna. Fossils are very abundant with many shells of lamellibranchs, gastropods and bryozoans (Fig. 7b). These carbonates are biomicritic, with wackestone-to-packstone textured, showing bivalve and microfilament sections. The carbonate series continues even in case of the absence of fauna (Fig. 7b). The thin section of these carbonates shows two varieties of texture, represented by micritic mudstone interrupted by biomicritic packstone ribbon, (Fig. 7d). The latter shows high concentration of bivalve sections (Fig. 8e). Limestones with mudstone textures are generally formed in shallow, quiet and open marine environments (distal platforms), indicating low hydrodynamic energy. The packstone ribbon is rich in bivalves are a result of a strong hydrodynamic regime, most probably caused by a storm event that brings bivalve fragments from shallow zones. If the environment returns to its initial state (low hydrodynamic energy), the micritic sedimentation reappears (mudstone texture). The series ends with an outcrop of marly clay grey, which is dolomitized with rare bivalve sections (Fig. 8f).

P.S: The phosphate deposits are intercalated between marls, clays, dolomites, and limestone of the Eocene Paleocene. The phosphate beam can reach 30 m in thickness with a homogeneous granulometry (≈250μm) of black and beige colors that are rich in glauconites characterizing the main layer of the Jebel Onk deposit. This layer also contains marly and dolomitic ores. From the mineralogical point of view, the phosphate ores consist of carbonate-fluoride apatite, and sometimes hydroxyapatite. The mineralogical composition of the apatite phase does not change between different locations except for the cement which varies from one facies to another, where dolomite and calcite are the most abundant minerals and are well recognized (Boulemia et al. 2021).

Ypresian: Brown dolomitic marly limestone with black flint and yellowish-white breakage, rich in bivalves (Fig. 7c) and traces of phosphate at the bottom. The microfacies show biomicritic mudstone-to-wackestone textures with bivalve and gastropod sections, as well as microfilaments (*Posydonomia*) (Fig. 8g).

Lutetian: According to the notice of the map of Bir El Ater N°327, scale: 1/50 000, investigation and field validation, it is a white gypsum formation well-bedded, interspersed with banks of dolomites and limestone.

Source: Authors' own study

Fig. 7. a) Maastrichtian flint limestone of the J. Zraga (Algerian-Tunisian border). b) Dano-Montian marly clays and limestones: Outcrop in the region of Hr. Halloufa in the proximity of Oued El Bir. c) Panoramic photo showing Maastrichtian flint limestones (J. Mrata), Ypresian dolomitic marly limestones and flint limestones (J. FedjEnnahla) and Miocene sands and clays. d) Miocene approximately W. El Horchane, from bottom to top: Conglomerates and clays, lagoonal gypsum formation, and lacustrine limestones with black flint deposits (e)

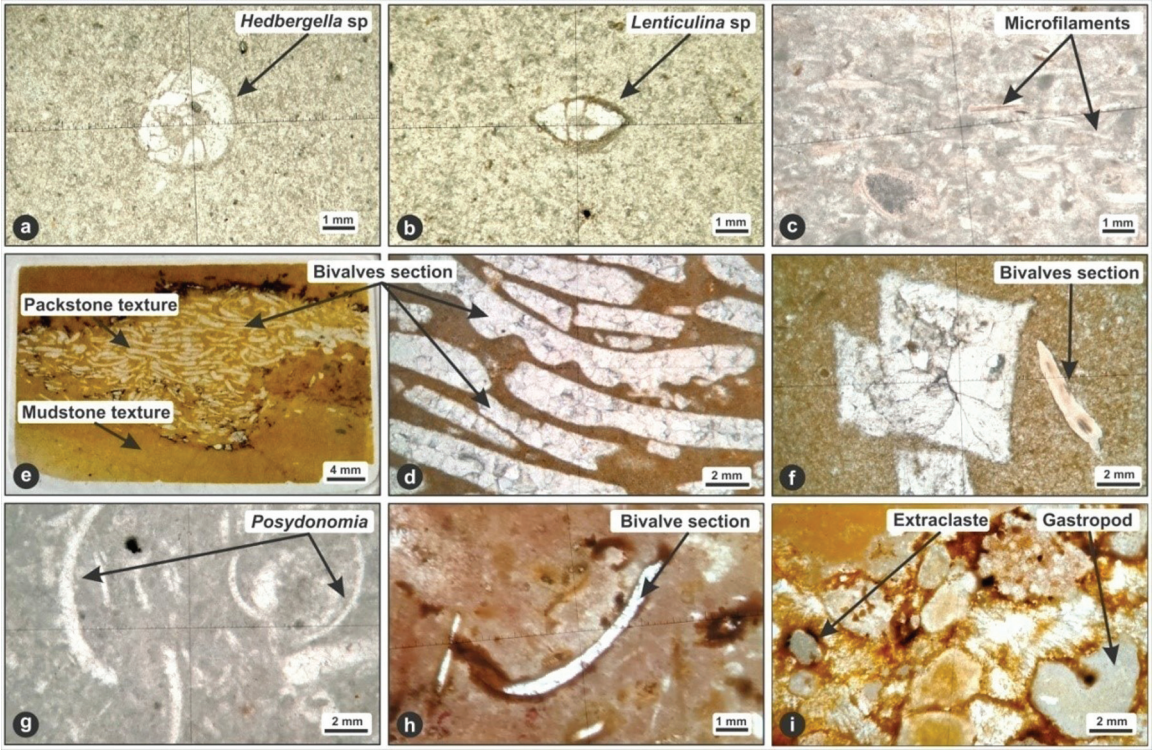

Source: Authors' own study

Fig. 8. Photomicrographs of some thin sections: a–b) Mudstone texture of the J. Zraga limestone with foraminifera (a: planktonic – Hedbergella sp., b: benthic – lenticulina sp.). c) dolomitized marly clay with rare bivalve section. d–e) Micritic mudstone interrupted by biomicritic packstone ribbon with concentration of bivalve section. f) Biomicritic wackestone-to-packstone texture with microfilaments. g) Mudstone-to-wackestone texture with bivalves sections and microfilaments. h–i) Packstone texture showing a section of gastropods, and bivalves

Mio-Plio-Quaternary: The series of Miocene begins with a thick conglomeratic layer which reshapes black flints, and is followed by a green gypsum lagoon formation that sometimes contains white-yellowish sandy clays (Fig. 7d). At the top of series, there are orange lacustrine limestones, the microfacies characterized by packstone texture with numerous benthonic faunas, represented b gastropods, bivalves, and corals. The texture shows also sub-rounded to sub-angular detritic grains, (Fig. 8h and i). The MPQ is characterized by sets of sandy clays and sandstone cover in the entire flat land of the sheet. With the appearance of conglomerates with black flint (Fig. 8d). There is also the massive white calcareous crust surmounting the formations said previously. Ancient and recent glaciers cover vast surfaces; they are accumulations of debris and the remains of past industries. The screes develop at the foot of the escarpments of the very diaclastic maastrichtian limestones of the J. Onk (Fig. 9).

Alluviums: Represented by sands, gravels, silts and pebbles located in the major beds of wades.

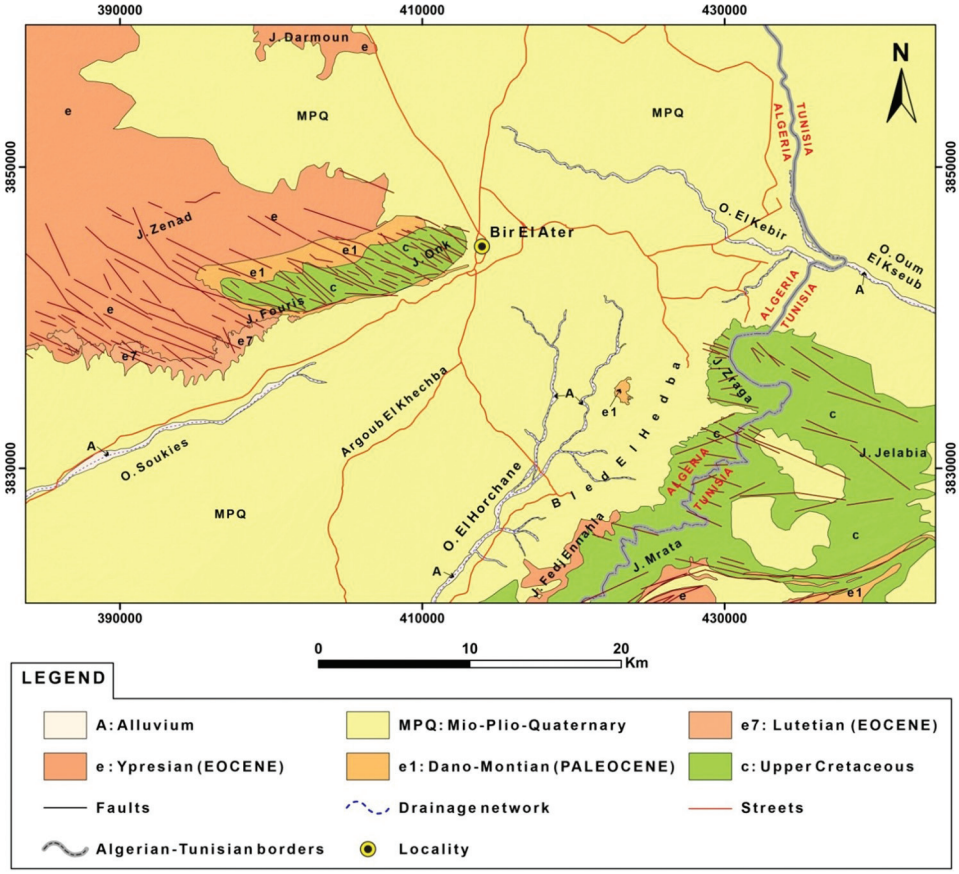

Source: Authors' own study

Fig. 9. Lithological map of the study area

6. Conclusion

The study involves applying the RS/GIS techniques to multispectral images. It begins with the preprocessing stage (radiometric calibration, atmospheric correction...), which is followed by various data analysis procedures and unsupervised classification. It was supported with fieldwork, which allowed us to discriminate well the major lithological sets in the study area. The lithological mapping using spatial data, associated with the analysis of the relief and assessed by the fieldwork, has allowed delineation of the contours of geological formations, while reducing the time and cost of research. These data cover a diversified geological terrain, with limestones and marls from the Upper Cretaceous to the Eocene in the J. Onk massif in the center of the mapped area, J. Zraga, J. Mrata... in the southeast. Conglomerates, clays and sand sub-tabular cover a large part of the map of the MPQ, as well as alluvial planes that contain eroded material from the surrounding hills. The results show a similarity between the image products of the two types of Landsat 8 OLI and Sentinel-2A multispectral images and the actual formations found in the field by our research team. Small differences are related to the spectral nature of the sensors.

References

Achour Y., Boumezbeur A., Hadji R., Chouabbi A., Cavaleiro V., Bendaoud E.A. 2017. Landslide susceptibility mapping using analytic hierarchy process and information value methods along a highway road section in Constantine, Algeria. Arabian Journal of Geosciences, 10(8), 1–16.

Alley R. 1999. Algorithm theoretical basis document for: decorrelation stretch.

Anis Z., Wissem G., Riheb H., Biswajeet P., Essghaier G.M. 2019. Effects of clay properties in the landslides genesis in flysch massif: Case study of Aïn Draham, North Western Tunisia. Journal of African Earth Sciences, 151, 146–152.

Boulemia S., Hadji R., Hamimed M. 2021. Depositional environment of phosphorites in a semiarid climate region, case of El Kouif area (Algerian-Tunisian border). Carbonates and Evaporites, 36(3), 1–15.

Dahoua L., Yakovitch S.V., Hadji R.H. 2017. GIS-based technic for roadside-slope stability assessment: an bivariate approach for A1 East-west highway, North Algeria. Mining Science, 24.

Demdoum A., Hamed Y., Feki M., Hadji R., Djebbar M. 2015. Multi-tracer investigation of groundwater in El Eulma Basin (Northwestern Algeria), North Africa. Arabian Journal of Geosciences, 8(5), 3321–3333.

El Fels A.E.A., El Ghorfi M. 2022. Using remote sensing data for geological mapping in semiarid environment: a machine learning approach. Earth Science Informatics, 15(1), 485–496.

El Mekki A., Hadji R., Chemseddine F. 2017. Use of slope failures inventory and climatic data for landslide susceptibility, vulnerability, and risk mapping in souk Ahras region. Mining Science, 24.

Fal S., Maanan M., Baidder L., Rhinane H. 2019. The contribution of Sentinel-2 satellite images for geological mapping in the south of Tafilalet basin (Eastern Anti-Atlas, Morocco). The International Archives of Photogrammetry, Remote Sensing and Spatial Information Sciences, 42, 75–82.

Gadri L., Hadji R., Zahri F., Benghazi Z., Boumezbeur A., Laid B.M., Raïs K. 2015. The quarries edges stability in opencast mines: a case study of the Jebel Onk phosphate mine, NE Algeria. Arabian Journal of Geosciences, 8 (11), 8987–8997.

Ge W., Cheng Q., Jing L., Armenakis C., Ding H. 2018. Lithological discrimination using ASTER and Sentinel-2A in the Shibanjing ophiolite complex of Beishan orogenic in Inner Mongolia, China. Advances in Space Research, 62(7), 1702–1716.

Green A.A., Berman M., Switzer P., Craig M.D. 1988. A transformation for ordering multispectral data in terms of image quality with implications for noise removal. IEEE Transactions on Geoscience and Remote Sensing, 26(1), 65–74.

Hadji R., Achour Y., Hamed Y. 2017a. Using GIS and RS for slope movement susceptibility mapping: comparing AHP, LI and LR methods for the Oued Mellah Basin, NE Algeria. In: Euro-Mediterranean Conference for Environmental Integration. Springer, Cham, 1853–1856.

Hadji R., Limani Y., Demdoum A. 2014 b. Using multivariate approach and GIS applications to predict slope instability hazard case study of Machrouha municipality, NE Algeria. In: 2014 1st International Conference on Information and Communication Technologies for Disaster Management (ICT-DM). IEEE, 1–10.

Hadji R., Limani Y., Baghem M., Demdoum A. 2013. Geologic, topographic and climatic controls in landslide hazard assessment using GIS modeling: a case study of Souk Ahras region, NE Algeria. Quaternary International, 302, 224–237.

Hadji R., Limani Y., Boumazbeur A.E., Demdoum A., Zighmi K., Zahri F., Chouabi A. 2014a. Climate change and its influence on shrinkage-swelling clays susceptibility in a semi-arid zone: a case study of Souk Ahras municipality, NE-Algeria. Desalination and Water Treatment, 52(10–12), 2057–2072.

Hadji R., Rais K., Gadri L., Chouabi A., Hamed Y. 2017b. Slope failure characteristics and slope movement susceptibility assessment using GIS in a medium scale: a case study from Ouled Driss and Machroha municipalities, Northeast Algeria. Arabian Journal for Science and Engineering, 42(1), 281–300.

Hamad A., Hadji R., Bâali F., Houda B., Redhaounia B., Zighmi K., Hamed Y. 2018. Conceptual model for karstic aquifers by combined analysis of GIS, chemical, thermal, and isotopic tools in Tuniso-Algerian transboundary basin. Arabian Journal of Geosciences, 11(15), 1–16.

Hamad A., Hadji R., Boubaya D., Brahmi S., Baali F., Legrioui R., Hamed Y. 2021. Integrating gravity data for structural investigation of the Youkous-Tebessa and Foussana-Talah transboundary basins (North Africa). Euro-Mediterranean Journal for Environmental Integration, 6(2), 1–11.

Hamed Y., Ahmadi R., Hadji R., Mokadem N., Dhia H.B., Ali W. 2014. Groundwater evolution of the Continental Intercalaire aquifer of Southern Tunisia and a part of Southern Algeria: use of geochemical and isotopic indicators. Desalination and Water Treatment, 52(10–12), 1990–1996.

Hamed Y., Khelifi F., Houda B., Sâad A.B., Ncibi K., Hadji R., Hamad A. 2022. Phosphate mining pollution in southern Tunisia: environmental, epidemiological, and socioeconomic investigation. Environment, Development and Sustainability, 1–18.

Hamed Y., Redhaounia B., Sâad A., Hadji R., Zahri F., Zighmi K. 2017. Hydrothermal waters from karst aquifer: Case study of the Trozza basin (Central Tunisia). Journal of Tethys, 5(1), 33–44.

Hammad N., Djidel M., Maabedi N. 2016 . Geological lineament mapping in arid area by semi-automatic extraction from satellite images: example at the El Kseïbat region (Algerian Sahara). Estudios Geologicos (Madrid), 72(1).

Khan S., Abbas A. 2007. Using remote sensing techniques for appraisal of irrigated soil salinity. Int. Congr. Model. Simul. (MODSIM), Model. Simul. Soc. Aust. New Zealand, Bright, (January), 2632–2638.

Lu J., Han L., Zha X., Li L. 2022 . Lithology classification in semi-arid areas based on vegetation suppression integrating microwave and optical remote sensing images: Duolun County, Inner Mongolia Autonomous Region, China. Geocarto International, 1–24.

Manchar N., Benabbas C., Hadji R., Bouaicha F., Grecu F. 2018. Landslide susceptibility assessment in Constantine region (NE Algeria) by means of statistical models. Studia Geotechnica et Mechanica, 40(3), 208–219.

Mokadem N., Demdoum A., Hamed Y., Bouri S., Hadji R., Boyce A., Sâad A. 2016. Hydrogeochemical and stable isotope data of groundwater of a multi-aquifer system: Northern Gafsa basin – Central Tunisia. Journal of African Earth Sciences, 114, 174–191.

Mouici R., Baali F., Hadji R., Boubaya D., Audra P., Fehdi C.É., ... Arfib B. 2017. Geophysical, Geotechnical, and Speleologic assessment for karst-sinkhole collapse genesis in Cheria plateau (NE Algeria). Mining Science, 24, 59–71.

Ncibi K., Hadji R., Hamdi M., Mokadem N., Abbes M., Khelifi F., ... Hamed Y. 2020. Application of the analytic hierarchy process to weight the criteria used to determine the Water Quality Index of groundwater in the northeastern basin of the Sidi Bouzid region, Central Tunisia. Euro-Mediterranean Journal for Environmental Integration, 5(1), 1–15.

Rais K., Kara M., Gadri L., Hadji R., Khochmen L. 2017. Original approach for the drilling process optimization in open cast mines: case study of Kef Essenoun open pit mine Northeast of Algeria. Mining Science, 24.

Shebl A., Kusky T., Csámer Á. 2022. Advanced land imager superiority in lithological classification utilizing machine learning algorithms. Arabian Journal of Geosciences, 15(9), 1–13.

Shirmard H., Farahbakhsh E., Müller R.D., Chandra R. 2022. A review of machine learning in processing remote sensing data for mineral exploration. Remote Sensing of Environment, 268, 112750.

Tamani F., Hadji R., Hamad A., Hamed Y. 2019. Integrating remotely sensed and GIS data for the detailed geological mapping in semi-arid regions: case of Youks les Bains Area, Tebessa Province, NE Algeria. Geotechnical and Geological Engineering, 37(4), 2903–2913.

Zahri F., Boukelloul M.L., Hadji R., Talhi K. 2016. Slope stability analysis in open pit mines of Jebel Gustar career, NE Algeria – a multi-steps approach. Mining Science, 23.

PhD Abdelmouhcene Chibani
Emergent Materials Research Unit, Farhat Abbas University, Algeria
Department of Earth Sciences, Institute of Architecture and Earth Sciences,
Ferhat Abbas University, Algeria
e-mail: abdelmouhcene.chibani@univ-setif.dz

Prof. Riheb Hadji
Department of Earth Sciences, Institute of Architecture and Earth Sciences, Ferhat Abbas University, Algeria
Laboratory of Applied Research in Engineering Geology, Geotechnics, Water Sciences, and Environment, Ferhat Abbas University, Algeria
e-mail: hadjirihab@yahoo.fr
ORCID: 0000-0002-9632-0812

Prof. Hamed Younes
Earth Sciences, Faculty of Sciences, University of Gafsa, Tunisia
e-mail: hamed_younes@yahoo.fr